ACS APPLIED MATERIALS & INTERFACES

www.acsami.org

Research Article

Assembly of Guanine Crystals as a Low-Polarizing Broadband Multilayer Reflector in a Spider, *Phoroncidia rubroargentea*

Jinjin Zhong, Zhengyong Song, Long Zhang, Xiang Li, Qingzu He, Yuer Lu, Sarah Kariko, Peter Shaw, Liyu Liu, Fangfu Ye,* Ling Li,* and Jianwei Shuai*

Cite This: *ACS Appl. Mater. Interfaces* 2022, 14, 32982–32993

Read Online

ACCESS | Metrics & More | Article Recommendations | Supporting Information

ABSTRACT: The diminishing of the polarization effect is important in the applications of dielectric multilayer reflectors in many optical systems, such as low-loss broadband waveguides, optical fibers, and LEDs. Low-polarizing broadband reflections were identified from birefringent-guanine-crystal-based multilayer reflectors in the skins of some fish. Previous models for these intriguing natural optical phenomena suggested the combined action of two populations of guanine crystals with an orthogonal low-refractive-index optic axis. Here we report a novel realization of polarization-insensitive broadband reflectivity in a spider, *Phoroncidia rubroargentea*, based solely on the type of guanine crystals with the low-refractive-index optic axis normal to the crystal plates. We examined the three-dimensional structure of the guanine assembly in the spider and performed finite-difference time-domain (FDTD) optical modeling of the guanine-based multilayer reflector. Comparative modeling studies reveal that the biological selection of the guanine crystal type and specific spatial arrangement work synergistically to optimize the polarization-insensitive broadband reflection. This study demonstrates the importance of both crystallographic characteristics and 3D arrangement of guanine crystals in understanding relevant natural optical effects and also provides new insights into similar broadband, low-polarizing reflections in biological optical systems. Learning from relevant biofunctional assembly of guanine crystals could promote the bioinspired design of nonpolarizing dielectric multilayer reflectors.

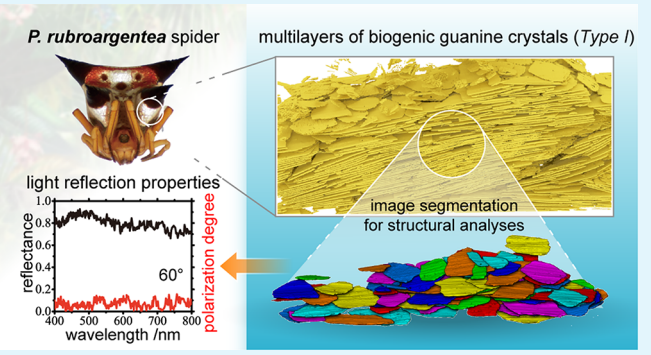

KEYWORDS: *biogenic assembly of guanine crystals, highly birefringent material, spatial arrangement, crystallographic characteristics, high reflectance and polarization-insensitive reflection*

1. INTRODUCTION

All dielectric multilayer as light reflectors, compared with metal or metal-dielectric multilayer reflectors, are low-loss and routinely used for optical utility requiring high reflectivity.[1] In nature, dielectric multilayer reflectors are widely used by different biological systems to realize multiple optical performance-based biofunctions, such as structural coloration for communication, mating displays or camouflage, and vision enhancement.[2] In practical applications, a key limitation of dielectric multilayer reflectors stems from the polarization effect on the non-polarized light source, which causes the decrease of the total reflectivity with increasing incidence angles of light.[3,4] Aside from the well-known magneto-optic materials[5] and polarizing beamsplitters,[6] the polarization effects are typically undesirable, as they constrain the angular performance of the multilayer reflectors. Researchers found that to adapt to optimal camouflage, some fish have evolved to develop their multilayer reflection systems in the skin or surface to produce low-polarizing broadband reflections.[7] These multilayer reflection systems are composed of alternating layers of birefringent biogenic guanine crystals separated by cytoplasm. Previous studies suggested that the diminishing of the polarization effect derives from the combined action of two populations of biogenic guanine crystals that have an orthogonal low-index optic axis.[7−10] In this study, we report a novel realization of the diminishing of the polarization effect in a more efficient way in a spider, *Phoroncidia rubroargentea*, with only one type of guanine crystal involved.

Guanine, one of the common metabolites from nucleic acid degradation processes in many animals, either converts into xanthine with guanase enzymes or is secreted as a waste product in organisms with relevant secretory control.[11,12] In

Received: May 30, 2022
Accepted: July 5, 2022
Published: July 14, 2022

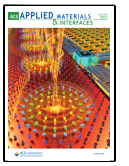

https://doi.org/10.1021/acsami.2c09546
ACS Appl. Mater. Interfaces 2022, 14, 32982−32993

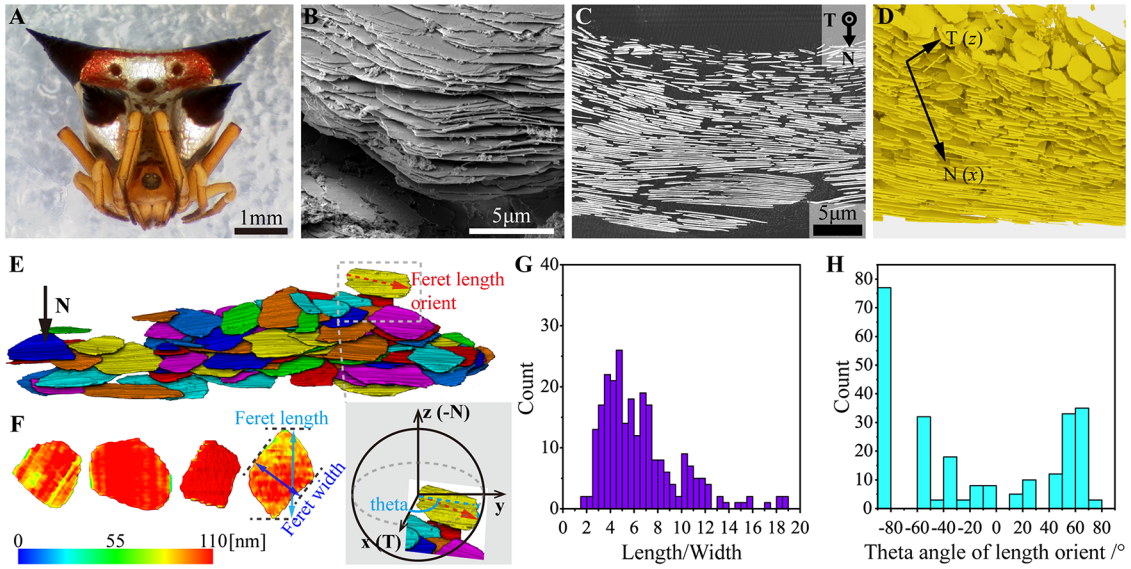

Figure 1. Morphologies of the guanine crystals and arrangement characteristics of the crystal assembly in the guanine−cytoplasm multilayered silvery reflection system in the spider *Phoroncidia rubroargentea* (Berland, 1913). (A) Photo of a *Phoroncidia* spider specimen. (B) A scanning electron microscopy (SEM) image of the multiple layers of guanine crystals in an individual guanocyte from the silvery region of the *Phoroncidia* spider sample. (C) One representative cross-section SEM image of the physical slices obtained by the microtome technique of the guanine crystal arrays in a localized region of the silvery abdomen site. T and N indicate the sectioning direction in microtoming and the normal direction of the cuticle surface, respectively. (D) 3D volume rendering of the guanine crystals in a localized region packed with the guanine−cytoplasm multilayer. (E) An exemplified region demonstrating the random stagger arrangement of the guanine microplates between adjacent layers. The inset shows the *xyz* coordinate (by correspondence with the N and T directions in panel C) used for the quantitative characterization on the theta angle of the Feret length orientation. The red dashed line indicates the Feret length orientation. The theta angle is the angle between the positive *x* axis and the projection of the length orientation to the *xy* plane. (F) Demonstration of 3D morphologies of some individual guanine crystals. The color bar indicates the thickness of the platy guanine crystals measured in nanometers. The schematic diagram for the Feret length and width is also shown using a guanine crystal plate. (G) Statistics on the ratio of length to width of the sampled guanine crystals. (H) The statistic on the theta angle of the thin plate length orientation of the sampled guanine crystals. The coordinate system is the same as the *xyz* coordinate system in panel E.

particular, microcrystalline deposits of guanine have been identified as a fixed end product in various tissues of 3 phyla out of all the 33 phyla, that is, Chordata, Arthropoda, and Mollusca.[2] These biological systems have developed various strategies to control the size, geometry, crystallography, and assembly of the guanine crystals for various optical functions, such as diffuse scatters, broadband reflectors, and tunable photonic crystals.[13−15] In particular, plate-like guanine microcrystal arrays intermediated by cytoplasm have been found in the skins of many fish and spiders for their silvery reflection[13,16] and in the sapphirinid copepods and some fish to produce tunable structural colors.[17,18] The primary biological functions for these optical effects are believed to be related to communication or camouflage.[16,17,19−21] Moreover, platy guanine crystals have also been identified in the tapetum of some fish eyes to enhance vision in dark living environments[22,23] and of some spider eyes as polarizers.[24,25]

Biofunctional assemblies of guanine crystals have function-adaptable morphologies, spatial arrangement, and crystallographic characteristics. Understanding the assembly−function relation is important for bioinspired designs and fabrications. In the guanine-based reflection systems, the guanine crystals have been identified to be in plate shapes. The geometry of these plate-like guanine crystals varies for different biological optical systems. The spatial arrangement of the crystals can also differ largely ranging from long-range ordered to locally ordered to disordered states. Narrow-band reflections are related with regularly shaped guanine crystals arranged in order, such as the aligned hexagons in the sapphirinid copepods[17,21,26] and the aligned squares in the eyes of scallops.[22] Broadband silvery reflections are originated from the multilayers composed of guanine crystals that exhibit local packing order but without long-range order. Platy guanine crystals of irregular hexagons were found in the reflecting iris of the zebrafish as well as in the silvery-colored scales of koi fish.[23,27] The guanine crystals from the reflection tissue underneath the integument of the silvery-colored spider *Tetragnatha montana* have no well-defined shapes.[28]

Despite the variations in crystal morphologies and assembly characteristics, biogenic guanine crystals that have been found in nature are all determined to be of anhydrous β polymorph (P1121/b, a = 3.59 Å, b = 9.72 Å, c = 18.34 Å, β = 119.5°).[29] In addition, the preferentially expressed face of these platy guanine crystals was identified in many organisms to be parallel to the hydrogen-bonding plane, i.e., the (100) plane.[2,29] This is quite different from the theoretically predicted preferred growth along the $\pi-\pi$ stacking direction perpendicular to the (100) plane, which has also been demonstrated in in vitro experiments.[14,29−31] Due to the highly anisotropic crystal structure, the refractive indices of guanine crystals along different crystallographic orientations are dramatically different, with the lower refractive index of ∼1.46 along the molecular stacking direction and the higher refractive index of ∼1.83 in the (100) plane.[2] It is generally believed that the preferential expression of the high-refractive-index (100) face was biologically selected by evolution to enhance the light reflection efficiency,[14] although the underlying molecular mechanism for such structural control is still under investigation.[32−36]

https://doi.org/10.1021/acsami.2c09546
ACS Appl. Mater. Interfaces 2022, 14, 32982−32993

For the silvery reflections, many previous investigations on the structure−property relation of these biological optical systems are based on simplified guanine−cytoplasm multilayer models utilizing idealized layering alignment to interpret the optical properties. Earlier studies treated the guanine crystals as optically isotropic materials and primarily focused on two aspects: the thickness of the guanine crystal plates and the cytoplasm spacing between the individual crystals.[16,37−40] The silvery reflection over the visible light was interpreted as a result of the variations of the thickness of guanine crystals, the cytoplasm spacing, or both.[8,39] In addition to the broadband and highly reflective properties, the silvery reflections from the surface of some fish were also identified to be of low polarization.[41,42] Based on simplified modeling with idealized layering alignment, Jordan et al. proposed an interesting optical model involving two populations of birefringent guanine crystals in the crystal stack. Each population has the low-index optic axis either perpendicular (type 1) or parallel to (type 2) the crystal plane.[7] With a certain ratio of the two types of guanine crystals and repeating such stack units in piles, the silvery reflection with low polarization can be achieved. In the latter relevant studies,[8,9] the low-polarized silvery reflection from the guanine crystal-based multilayers has always been dependent on the presence of the type 2 guanine crystals. This work demonstrates how the multilayer reflection system in a spider realizes low-polarizing broadband silvery reflections only with the type 1 guanine crystals.

In this work, we examined the assemblies of the guanine microplatelets from the silvery abdomen of a spider, *Phoroncidia rubroargentea* (Berland, 1913),[43] and investigated the optical performance of this system through a systematic finite-difference time-domain (FDTD) optical modeling.[44] The 3D assembly of individual guanine microplates was first obtained by utilizing a tomography method enabled by the combination of serial sectioning and high-resolution electron microscopy imaging. The structural characterizations reveal that the individual guanine microplates exhibit irregular peripheral profiles and local randomness in the assembly. The guanine crystals are much smaller and more randomly arranged in the interior region of the guanocytes. Toward the edge side of the cells, larger guanine crystals are more closely packed and tend to be aligned alongside the edge of the cells. Based on the original structure, we conducted systematic FDTD optical modeling compared to simplified models with ideally aligned guanine microplates. Our results suggest that in this natural guanine assembly system, the type 1 crystallographic alignment together with the randomly staggered arrangement works synergistically to enhance the reflectance and, more importantly, to reduce the polarization across the visible light range at wide viewing angles. This study provides a new understanding of the low-polarization silvery reflection from natural guanine crystal-based optical systems in contrast to the necessity of the presence of type 2 guanine crystal.[7] This study also indicates the importance of the knowledge of 3D structural and crystallographic characteristics of the guanine assembly both for correctly understanding the structure−function relation in relevant biological optical systems and for bioinspired designs and fabrications.

2. RESULTS

2.1. The Assembly Structure of Guanine Microplatelets in 3D. The model spider in this study, *Phoroncidia rubroargentea* (Berland, 1913), belongs to the family of Theridiidae and is small (∼3 mm) and vibrantly colored (red, silver, and black). It can be typically found in the rainforest in Madagascar. Figure 1A shows a specimen photo of the *P. rubroargentea* spider. The structural origins of coloration in this spider have been elaborately described in the previous work. The prominent silvery appearance of its abdomen was determined to originate from the guanine−cytoplasm multilayers in the guanocytes underlying the transparent cuticle.[43] Figure 1B shows a scanning electron microscopic (SEM) image of the multilayered assembly of guanine microplates from a guanocyte.

Similar to other studies, our previous structural analysis on the guanine-based biological optical structure was based on two-dimensional characterizations.[43] Here, we conducted quantitative 3D structural characterizations on the guanine crystals in the silvery region. To obtain the 3D morphology of individual guanine crystals and their assembly structure, we utilized the automatic serial microtome-sectioning and subsequent electron microscopic imaging of the guanine−cytoplasm multilayer structure. Figure 1C shows the SEM image of one representative cross section of a guanocyte packed with guanine crystals, where the N and T direction represents the normal and tangential direction of the cuticle, respectively. 3D reconstruction allows us to examine the characteristics of the morphology of the guanine crystals and the arrangement of the assembly in more detail.

Based on image segmentation and 3D volume and surface rendering, individual guanine crystals can be isolated for quantitative shape analyses. The thickness of the guanine crystals is 110.7 ± 22.8 nm (n = 134, where n is the total number of the guanine crystals sampled for statistics here) (Figure 1F), consistent with previous 2D measurements.[43] The individual crystals sampled from the multilayer (Figure 1E,F) exhibit irregular peripheral profiles with no well-defined or conserved morphology like the square- or hexagon-shaped guanine crystals in some biological systems,[2,17] demonstrating less biological control in the in-plane development. The Feret length and width were used to characterize the largest and smallest dimensions of the microplate plane (Figure 1F). A statistic on the Feret length/width ratio shows a large span (Figure 1G), further demonstrating the irregular shapes in the crystal plane dimension. In the previous work on this spider,[43] crystallographic analyses based on electron diffractions demonstrated that these guanine crystals are type 1 with (100) as the plate surface, similar to many other biogenic guanine microplate-based optical systems.[14,45]

Compared with those regularly packed guanine crystals in some biological systems, the spatial arrangement of the guanine assembly presents a typical self-assembly pattern rather than a precise biological control. In the inner rows of the multilayers in the guanocytes, smaller guanine crystals are more loosely packed and randomly distributed. Larger guanine crystals are more densely packed toward the edge side of the cells and tend to be aligned alongside the local cell contour. More structural details on the assembly of the biogenic guanine crystals in this spider reflection system are provided in Figure S1. According to the crystallographic characteristics of the guanine microplates, the three crystallographic axes of guanine crystals are orthogonal.[2] Two crystallographic axes lie parallel to the plate face of the microplates, and one is along the normal direction of the microplates. We made a quantitative characterization on the normal direction of the guanine crystals by the statistic on the normal direction of each

https://doi.org/10.1021/acsami.2c09546
ACS Appl. Mater. Interfaces 2022, 14, 32982−32993

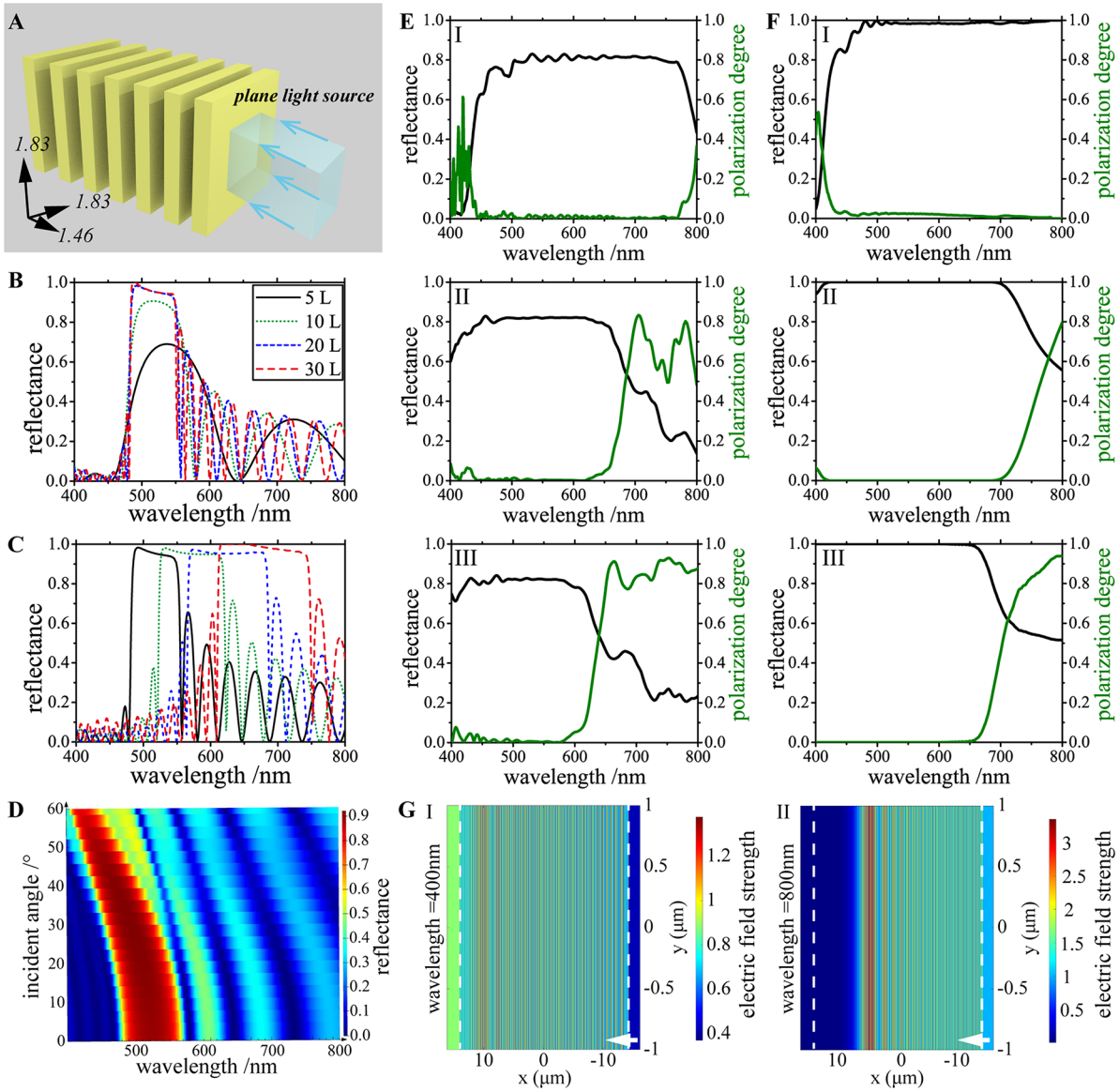

Figure 2. Simulated reflections of the guanine−cytoplasm multilayers using simplified models. (A) Schematic of the geometrical setup in the simulations. The yellow plate arrays are the guanine crystals 110 nm thick with an intermediating space filled with water, representing the cytoplasm in the guanocytes. The layer number of the guanine−cytoplasm arrays or the cytoplasm spacing between them varies in different simulation cases. (B) Reflectance spectra for cytoplasm spacing ∼40 nm for 5 (black line), 10 (green line), 20 (blue line), and 30 (red line) layers, respectively, with perpendicularly incident light. (C) Reflectance spectra for layer number ∼20 and cytoplasm spacing ∼40 nm (black line), ∼60 nm (green line), ∼80 nm (blue line), and ∼100 nm (red line), respectively. (D) Angular dependence of reflectance spectra for the non-polarized light incident on the multilayer in which the cytoplasm spacing is ∼40 nm and the layer number ∼10. (E) Reflectance (black line) and polarization degree (green line) from the simplified model 1 for non-polarized light incident at 20° (I), 50° (II), and 60° (III). (F) Reflectance (black line) and polarization degree (green line) from the simplified model 2 for non-polarized light incident at 20° (I), 50° (II), and 60° (III). (G) Profiles of the electric field strength in the *xy* plane for *p*-polarized light at wavelength ∼400 nm (I) and ∼800 nm (II) for the case in I of panel F. The white arrows and the white dashed lines indicate the incident direction of light and the two boundaries of the multilayer stack of the simplified model 2, respectively.

individual crystal involved in the sampled original multilayer structure used in the optical modeling in Section 2.3. The statistical result shows that the normal direction of most of the crystals lies within a range from −20 to 20° in Section 2.3. Previous studies show that the long axes of guanine microplates are usually co-aligned with the principal crystallographic orientation along which the crystals prefer to grow.[14,15] Here, we use the angle (denoted as the theta angle) between the projection of the elongated direction (Feret length) on the *xy* plane and the *x* direction to represent the in-plane crystallographic orientations of a guanine microplate. The statistic on the theta angle of the Feret length orientation in Figure 1H indicates that the assembly of the guanine crystal plates seems to have a preferred elongation direction that is perpendicular to the T direction and has a roughly symmetric distribution at the two sides of the preferred direction. These analyses indicate that the guanine microplates are not stacked precisely on top of each other but exhibit morphological and orientation variations between adjacent crystals. One microplate can oppose two or more microplates from the adjacent layers (Figure 1D,E). The knowledge of the guanine assembly characteristics is important not only for investigating the

https://doi.org/10.1021/acsami.2c09546
ACS Appl. Mater. Interfaces 2022, 14, 32982−32993

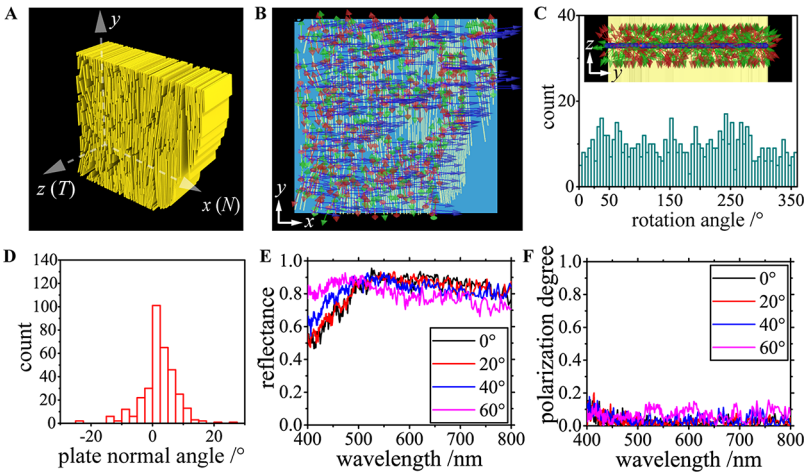

Figure 3. FDTD modeling of the reflections from the guanine−cytoplasm multilayer in the subject spider across the full visible wavelengths for different incidence angles. (A) The 3D geometry setup of the guanine material for the simulations, constructed from the original structures in Figure 1C. The intermediating spacing is filled with cytoplasm. (B−D) The setup of directions of the optic axes for each individual guanine crystal in the modeling, with a demonstration of the profile in the (B) *xy* plane and (inset in C) *yz* plane. The red and green arrows indicate the two high-index optic axes parallel to the large face of the microplates, and the blue arrows indicate the low-index optic axis, i.e., the normal direction of the microplates. Statistics on the rotation angle of the red arrows from *z* and on the angles of the blue arrows relative to the *x* axis are shown in panels C and D, respectively. (E, F) The calculated spectra of the (E) reflectance and the (F) polarization degree of the reflected light from the modeling with setups in panels A−D for non-polarized light incident at 0, 20, 40, and 60°.

related biofunctions but also for further studies of the assembly mechanism that remains unknown for now.

2.2. Optical Properties of the Idealized Multilayer Model. Having determined the guanine crystals' morphologies and the assembly's arrangement characteristics, we next investigated how the assembly of type 1 guanine microplatelets achieves the desired silvery reflection properties through systematic optical FDTD simulations. We first examined the optical performance of simplified guanine microplate−cytoplasm multilayer structures (Figure 2A) in which the crystal plates (110 nm thick) are parallel and placed in a stack periodically. Following the relationship between the refractive indices and the crystallographic orientations, the refractive index along the normal direction of the plates is ∼1.46, whereas the other two optical axes with a refractive index of 1.83 are parallel to the plates.[2] As the optical property of cytoplasm is close to water with a refractive index of ∼1.33, the intermediating component filling between the guanine crystals was set to be water in all the simulations in this work. With these simplified models, the effects of some structural factors on the optical performance of the guanine crystals in the subject system were evaluated, including the number of layers, cytoplasm spacing, and the angle of incidence of light. The polarization degree of the reflected light is defined as $|R_p - R_s|/(R_p + R_s)$, in which R_p and R_s represent the reflectance of *p*-polarized and *s*-polarized light component, respectively.

As shown in Figure 2B, only increasing the layer number of the guanine−cytoplasm multilayers narrows down the reflection band and enhances the reflectance within the reflection band. With increased cytoplasm spacing (from 20 to 100 nm), the highly reflective region shifts toward the larger wavelengths and becomes broader (Figure 2C). As the incidence angle relative to the crystal normal increases, the main reflection band tends to shift toward the shorter wavelengths for the non-polarized light source (Figure 2D). The shifting of the high-reflectance band is no more than 70 nm for a total inclination of 60°.

We further constructed two simplified models similar to previous relevant studies to investigate the optical performance of the guanine-based multilayer system but with only the type 1 guanine crystals involved. In the spider's multilayer structure as characterized in the above section, the thickness of the guanine crystals is relatively uniform at 110 nm, while the cytoplasm spacing varies largely. To cover the variation range of the cytoplasm spacing and the layer number of guanine crystals that is no more than 100 in the sampled natural multilayer structure in Figure 1C,D, we sampled across the thickness of cytoplasm spacing from 20 to 120 nm with a layer number of 100 (simplified model 1) and from 5 to 150 nm with a layer number of 150 (simplified model 2), respectively. In the simplified models 1 and 2, the cytoplasm spacing increases by 5 nm every five layers of guanine crystals. In this work, the layer number indicates the layer number of the guanine crystal plates in the guanine−cytoplasm multilayers. The spectra for the reflectance and the polarization degree were calculated under different incident angles for the simplified model 1 (Figure 2E) and model 2 (Figure 2F). When light hits onto the large guanine crystal face with an incident angle ∼20° relative to the plate normal direction, the reflections from these two models all demonstrate low reflectance at shorter wavelengths with high polarization degree (Figure 2E,F). When the incident angle increases, the low-reflectance spectral band always accompanied by high polarization degree here changes to the long wavelengths from the short wavelengths (Figure 2E,F). Figure 2G shows the color mapping of the electric field strength in the simplified model 2. The calculated electric field strength distributions at ∼400 and ∼ 800 nm in the simplified model 2 show agreement with their respective reflectance. Most of the light penetrate through the multilayer stack and only a very small fraction can be reflected for the wavelength ∼400 nm. The light propagation was totally prevented for the wavelength ∼800 nm before reaching the end of the multilayer stack, which results in 100% reflectivity. We also calculated the reflection behavior with a hypothetic optically isotropic nonbirefringent

https://doi.org/10.1021/acsami.2c09546
ACS Appl. Mater. Interfaces 2022, 14, 32982−32993

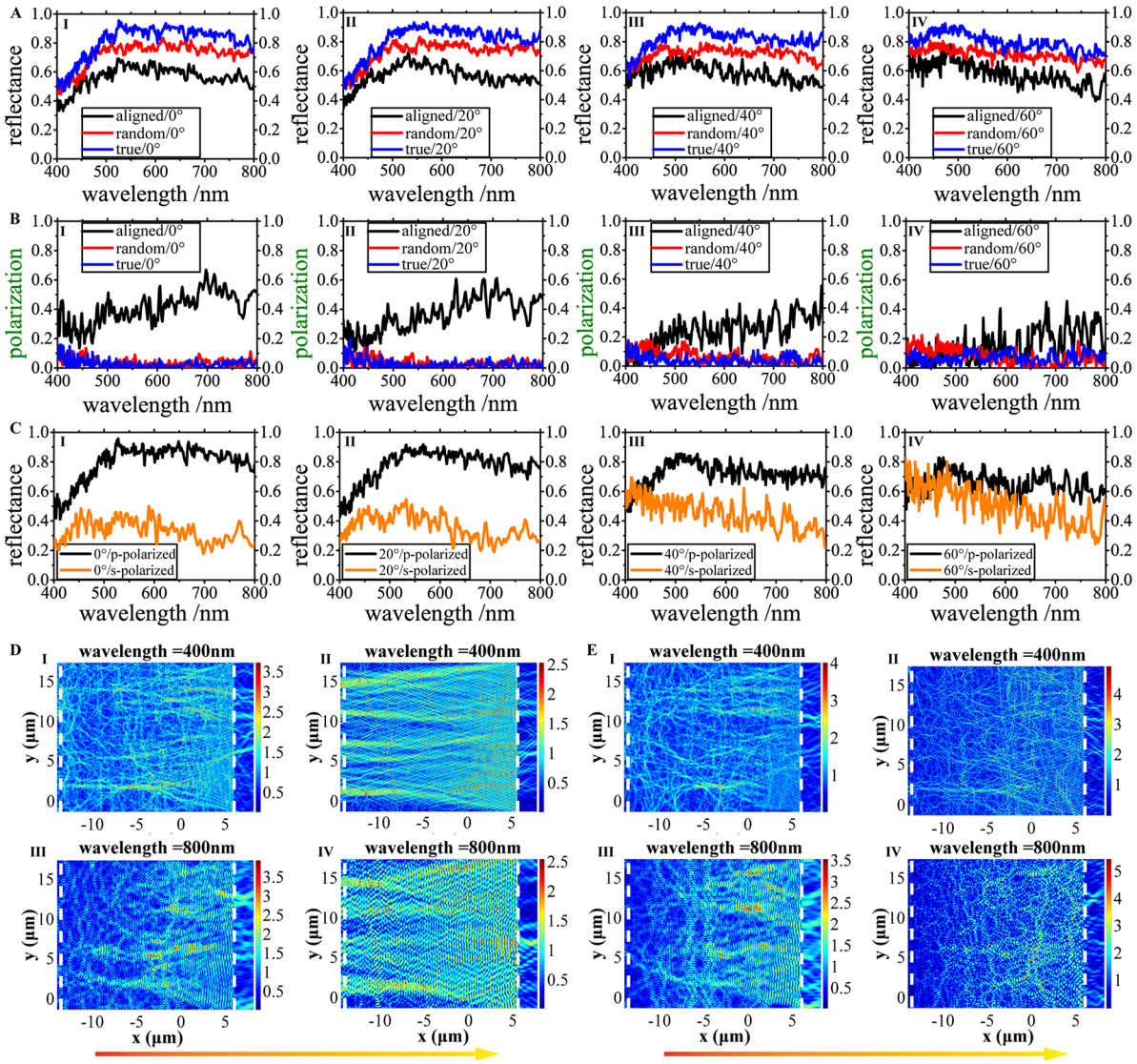

Figure 4. Comparison of the reflection performance of the guanine−cytoplasm multilayer in the subject spider under different birefringence distribution states. (A) The calculated reflectance spectra for the non-polarized source with an incident angle of 0° (I), 20° (II), 40° (III), and 60° (IV) from left to right panels, respectively, under the "aligned" (black lines) in-plane, "random" (red lines) in-plane, and the true birefringence distributions (blue lines). (B) The calculated spectra of the reflection polarization degree for an incident angle of 0° (I), 20° (II), 40° (III), and 60° (IV) from left to right panels, respectively, under the "aligned" (black lines) in-plane, "random" (red lines) in-plane, and the true birefringence distributions (blue lines). (C) The calculated reflectance spectra for *p*- (black lines) and *s*-polarized (orange lines) light with the incident angle of 0° (I), 20° (II), 40° (III), and 60° (IV) from left to right panels, respectively. (D, E) The calculated profiles of electric field in the cross section as in Figure 3B under the condition of (D) "aligned" in-plane and (E) true birefringence distribution at an incident angle of 0° for *p*- (I) and *s*-polarized (II) light of 400 nm and for *p*- (III) and *s*-polarized (IV) light of 800 nm, respectively. The arrows indicate the same N orientation as Figures 1 and 3. The color bar indicates the electric field strength. The white dashed lines indicate the boundaries of the multilayer structure.

state of the guanine component with an averaged refractive index at 1.65. Although the reflection behavior from the multilayer with the nonbirefringent guanine plates (Figure S2) is quite similar to the birefringent component of guanine crystal plates, birefringent guanine crystals perform better than the nonbirefringent state in the simplified models when the polarization effect is undesirable (Figure S3). Previous studies have led to a conclusion that the guanine-based multilayer unavoidably predicts a strong polarization effect with only type 1 guanine crystal. The calculated reflections for the two simplified models in this study both show spectral regions of high polarization degree and largely reduced reflectance, as concluded in numerous previous studies.[7,15,39,46,47]

2.3. Optical Properties of the Guanine Microplatelet Assembly in the Spider. 3D structural characterizations on the assembly of the guanine crystals in the model spider in Section 2.1 indicate a random staggering in the spatial arrangement. This characteristic in spatial arrangement was totally neglected in previous optical modeling. Here we conducted optical modeling based on the experimentally measured 3D assembly of guanine microplates to understand the reflection behavior from such a biological optical system. Figure 3A shows the 3D geometry model obtained from one sampled localized region of a guanocyte with complete guanine−cytoplasm structures. According to the optical characteristic of type 1 guanine crystal, the lower refractive index of ∼1.46 is along the normal direction of the microplates,

https://doi.org/10.1021/acsami.2c09546
ACS Appl. Mater. Interfaces 2022, 14, 32982−32993

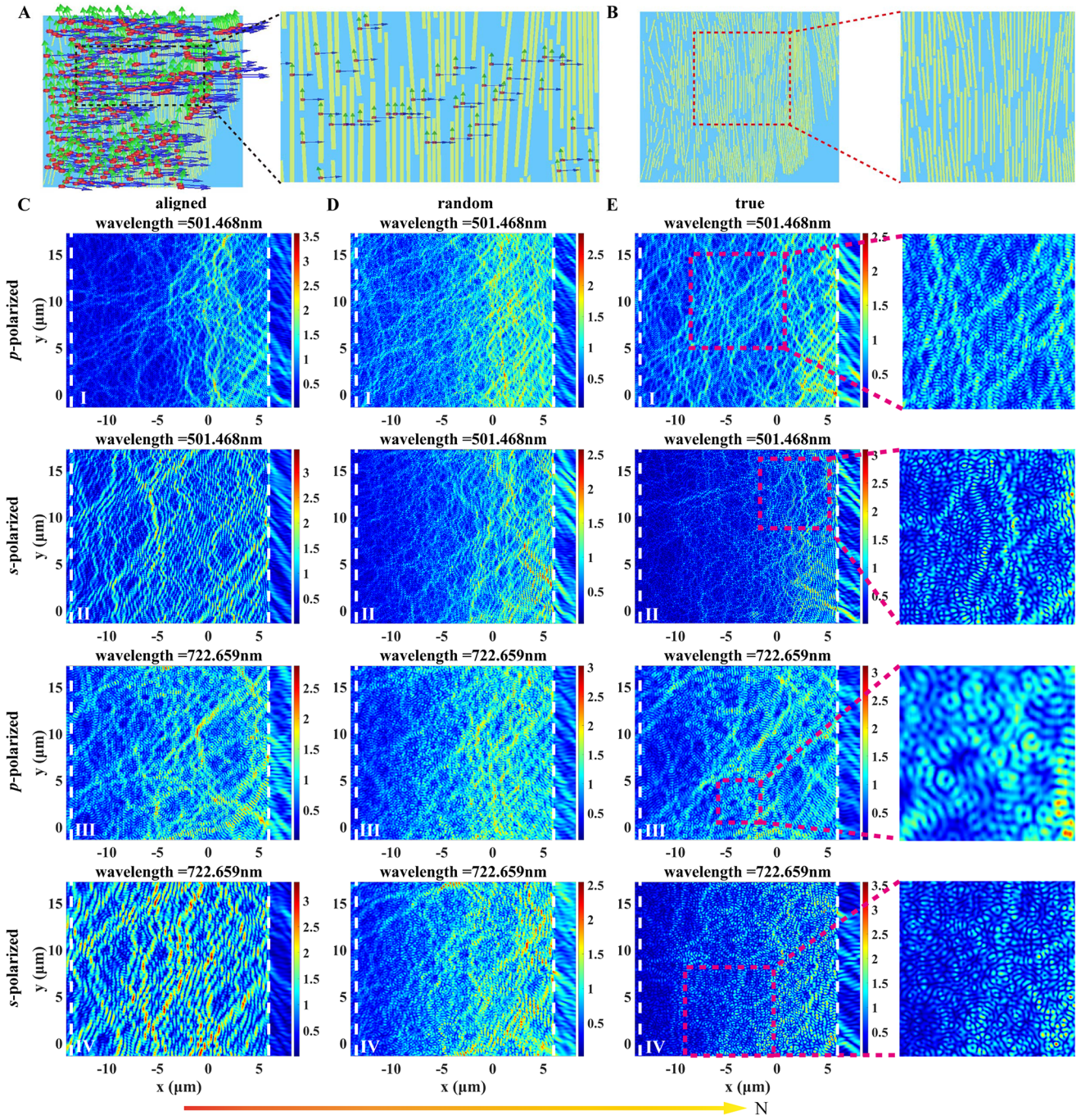

Figure 5. (A, B) The setups of (A) the crystallographic orientations and (B) the geometry of the involved guanine crystals in the optical modeling. The inset of panel A shows an enlarged image of the domain outlined by a black dashed square. The inset of panel B shows an enlarged image of the domain outlined by a red dashed square. (C, D) The calculated profiles of the electric field strength in the cross section as in panels A and B—and Figure 3B at an incident angle of 60° and wavelength of 501 nm of *p*-polarized (I) and *s*-polarized (II) light—of 722 nm of *p*-polarized (III) and *s*-polarized (IV) light (C) under ″aligned″ in-plane birefringence distribution, (D) under ″random″ in-plane birefringence distribution, (E) and under true birefringence distribution, with the right column showing the enlarged images of some exemplifying regions with the occurrence of localization of light. The arrow indicates the N orientation occurring in Figures 1 and 3. The color bar indicates the electric field strength. The white dashed lines indicate the boundaries of the multilayer structure.

and the other two optic axes with the higher refractive index of ∼1.83 are parallel to the crystal plane (Figure 3B). As the in-plane optical property is isotropic for the type 1 guanine crystal, we use a uniformly random distribution of the in-plane optic axes in the setup of the optical property of each guanine crystal to make a direct comparison with the following ″random″ model. Each guanine crystal was assigned with a random in-plane rotation angle between 0 and 360° for one of the two ordinary optic axes, as demonstrated in Figure 3C. The lower refractive index was precisely defined for each guanine crystal, which is set along the normal direction of the individuals. The distribution of the low-indexed normal direction of each individual crystal is shown in Figure 3D, which has been mentioned in the discussion of the guanine

https://doi.org/10.1021/acsami.2c09546
ACS Appl. Mater. Interfaces 2022, 14, 32982−32993

assembly characteristics in Section 2.1. With the more accurate structural model, the FDTD optical modeling results suggest that this multilayer system exhibits high reflectance over the visible wavelengths for a wide range of incident angles from 0 to 60° (Figure 3E). More importantly, these reflections also show a property of low polarization (lower than 0.2, Figure 3F), which is similar to the reflections that have been reported from the surface of some fish.[7,41,42]

Previous optical modeling of guanine crystal-based reflectors with the idealized layering alignment unavoidably predicts Fresnel polarization at Brewster's angle,[7,46] which was also confirmed in our modeling results (Figure 2E,F). This was resolved by introducing another set of guanine crystals (type 2) with their low-index optic axis parallel to the large crystal surface in the idealized multilayer modeling.[7] Our study shows that the optical effects of high reflectance with low polarization can be achieved only based on the type 1 guanine crystals but with experimentally observed microplate assemblies.

Compared with using simplified modeling, there is an essential difference in the requirement of the types of guanine crystals to realize the polarization-insensitive silvery reflection when considering the complexities in the original structure. Although simplified models cover the dynamic range of thickness variation of the cytoplasm spacing, one important difference that has been neglected in previous mechanism studies is the random stagger arrangement of the guanine microplates between adjacent layers caused by the variation of the sizes, morphologies, cytoplasm spacing, and orientations of the microplates. The essential difference in the requirement of the guanine crystal type to interpret low-polarization silvery reflections indicates the great importance of the 3D spatial arrangement in understanding the optical effects of guanine crystal-based optical elements.

2.4. Comparison with Two Hypothetic Structures. The effect of the crystallographic characteristics on the optical performance was further examined by comparative modeling studies. Two hypothetical models were constructed using the same geometrical setup as in Figure 3A obtained experimentally, while the guanine crystals are type 2. Compared with the ″true″ model, the crystallographic orientations of the guanine microplates were modified by orienting one of the high-index optic axes toward the microplate normal direction. The other two optic axes are parallel to the large face of the microplates. In the first hypothetical model (denoted as the ″aligned model″), each guanine crystal's low-index optic axis is always along the positive z direction. In contrast, in the second hypothetical model (denoted as the ″random model″), the orientations of the guanine microplates are orthogonal to the setup in Figure 3B−D. We also made a schematic diagram in Figure S4 to make it easier to understand the difference of the models for comparative studies.

The reflectance and polarization degree of the reflected light from the ″aligned″ and ″random″ models were calculated (Figure 4A−C). Compared with the reflections from the two hypothetic models, the biological selection of the guanine crystal type with the low-index optic axis along the normal direction of the guanine crystal microplates (the ″true″ model) could enhance the reflectance and reduce the polarization degree in the visible light range, optimizing the metallic-like silvery reflection. By replacing the birefringent guanine crystals with the hypothetic isotropic guanine component in optical properties (the refractive index is ∼1.65), the reflectance from the true structure is reduced (Figure S5) and the polarization degree is increased to a relatively high level, especially for large incidence angles (Figure S6). This comparison further demonstrates the advantage of the biological selection of the type 1 guanine crystals in diminishing the polarizing effect in the guanine assembly of the multilayer structures in the subject spider reflection system. In addition, the simulation results show that the reflection behavior from the ″aligned″ model exhibits the highest polarization degree and the lowest reflectance across the visible light range, in stark contrast to the ″true″ and the ″random″ models. The large difference in the reflection properties from the ″true″, ″aligned″, and ″random″ models indicates the importance of the knowledge of the birefringence distribution of the guanine crystals when studying the optical performance of such guanine crystals-involved systems. The results also suggest that the low polarization could not be achieved only by virtue of the structural arrangement of the guanine assembly but is the result of the cooperation with specific crystallographic characteristics of the individual guanine crystals. In addition, we also test the ″random″ model on the simplified model 2 as in Section 2.2. The simulation results shown in Figure S7 still demonstrate a relatively high polarization degree for some spectral ranges, which demonstrates that low polarization will not occur when only random crystallographic orientations exist, further indicating the importance of the knowledge of the 3D structural arrangement in investigating the optical performance of the related structure. The systematic comparisons indicate that the low-polarized silvery reflection is achieved as a synergistic effect of the spatial arrangement and crystallographic orientations.

To further understand the exceptionally high polarization of the reflected light from the ″aligned″ model, we examined the p- and s-polarized components in the reflection, respectively (Figure 4C). It was found that the reflectance of the s-polarized light was much lower than all the other situations, resulting in the highest polarization and lowest reflectance for unpolarized light in the ″aligned″ case. The calculated profiles reveal a significant difference in the propagation behavior of the s-polarized light under this ″aligned″ birefringence distribution state, as exemplified in Figure 4D,E. The localization of light[48] can frequently occur due to the appearance of local disorders for both p- and s-polarized light in the ″random″ and ″true″ models and the p-polarized light for the ″aligned″ model. The localization of light appears to rarely happen for the s-polarized source in the ″aligned″ model. From such a strong correlation, we assume that the localization of light might play an essential role in enhancing the reflectance. Figure 5 and Figures S8 and S9 provide more profiles of the electric field strength in the ″aligned″, ″random″, and ″true″ models for p- and s-polarized incident light. More details of such differences in the light propagation for different sources can be seen in the enlarged images in Figure 5C.

For the type 2 guanine crystals, the increased randomness of the in-plane crystallographic orientations can lead to an essential difference in the behavior of s-polarized light when propagating in the assembly structure of the guanine crystals in the subject spider. Compared with the ″aligned″ model, the light is inclined to be more intensively localized at various regions in the ″random″ model with the increase of the randomness of the in-plane crystallographic orientations (Figure 5C,D). With the same assembly structure, the reflected light is highly polarized for the ″aligned″ model, especially for the large incidence angles. In the ″aligned″ model, the p-

https://doi.org/10.1021/acsami.2c09546
ACS Appl. Mater. Interfaces 2022, 14, 32982−32993

polarized light performs better than the *s*-polarized light, and most of the *p*-polarized light can be reflected over a large range of incidence angles. From the electric field strength distribution in Figure 5E, it can be seen that despite the small difference in the ultimate reflectance between the *p*- and *s*-polarized light (Figure 4A,B) for the ″true″ model, the prevention of the propagation of the *s*-polarized light was mostly realized in the outermost region of large stacks of more regularly and densely packed guanine crystals of a larger size, especially for the shorter wavelength region. The smaller guanine crystals in the middle and innermost region also play an important role in the prevention of the light propagation for the *p*-polarized light in the ″true″ model. The *p*-polarized light was intensively localized in the more interior regions, while the *s*-polarized light was more intensively localized in the outermost region. The *s*-polarized light also performs better in the ″true″ model than in the ″random″ model in terms of reflection (Figure 5D,E), with only the change of the type of guanine crystals.

3. CONCLUSIONS AND DISCUSSION

This study identified a natural guanine crystal-based multilayer reflection system, which can reflect polarization-insensitive silvery color with only type 1 guanine crystals. First, we take advantage of serial microtoming and SEM imaging and obtain, for the first time, the 3D guanine crystal-based optical structure with nanometer resolution in the abdomen of the model spider *P. rubroargentea*. The reflection properties of high reflectance and low polarization were obtained by direct optical modeling based on the original structure of the guanine crystals in this system. This study examined the assembly of the guanine crystals in the multilayer reflector systems. A comparative study was performed on four different cases of the crystallographic orientations: the idealized model with strictly aligned guanine crystals, the ″true″ model with the type 1 guanine crystals, and the ″aligned″ and ″random″ models with type 2 guanine crystals. The study demonstrated that the low-polarized broadband reflection originated from (a) the biological selection of type 1 guanine crystals and (b) the structural arrangement of self-assembling-like random staggering, which exhibits larger randomness in the interior side of the cell and tends to be more aligned toward the edge side of the cell. The results show that the spatial arrangement and crystallographic distributions work synergistically to influence the reflection behavior. This natural reflection system has biologically selected the type of guanine crystals with the low-index optic axis along the normal direction of the microplates, together with the random stagger arrangement in assembly, to enhance the reflectance as well as to reduce the polarization degree. The localization of light was suggested to play an important role in realizing the polarization-insensitive silvery reflections. This silvery reflection is presumed to have developed as a disguise, as it appears similar to the sparkling water droplet in the rainforest environment.[49] The polarization-insensitive silvery reflection from the highly birefringent guanine crystal has been previously studied using simplified models based on periodically layered structures. In addition, the presence of type 2 guanine crystal with the low-index optic axis parallel to the large exposed surface was a necessity.[7−10] Optical modeling based on the original structure in the model spider in this study reveals an essential difference in the requirement of the guanine crystal type to realize the polarization-insensitive silvery reflection. The low-polarizing broadband reflections can be realized in this novel system in a more efficient way compared with previous models in terms of the requirement of both the layering number and the crystal type. This study indicates the importance of the knowledge of the 3D assembly and crystallographic characteristics in understanding the optical performance of a guanine crystal-based natural reflection system.

In view that only the type of the guanine crystal that has a high-refractive-index large surface was found in many similar silvery reflection systems, this work suggests that these biological systems may exploit the synergistic effect of the cooperation of the structural arrangement and the particular crystallographic characteristic to optimize the silvery reflections. Compared with exquisite control over the ratio of the two types of guanine crystals, the cooperation of biological control over the crystallographic orientation of the incorporated guanine crystals and self-assembly might be more energy cost-efficient and more favorable by relevant natural silvery reflection systems. Biogenic guanine crystals are widely employed in natural optical systems and are found with many different biofunctional assemblies. As a readily available organic material, the guanine crystal holds a great potential in applications in bioinspired optical devices due to its high refractive index and bio- and environmental compatibility. Understanding the assembly−function relation in relevant natural optical systems can promote bioinspired fabrications and designations of advanced optical devices.

4. MATERIALS AND METHODS

4.1. Sample Preparation and Image Acquisition. For this study, preserved museum specimens of *Phoroncidia rubroargentea* were examined from the collections of both the Museum of Comparative Zoology (MCZ) and the California Academy of Sciences (CAS) where they were stored in 70−80% ethanol (MCZ IZ 143122, 32022, 50966, 53933, and 54189; CASENT 9057540, 9003201, 9057570, 9057533, 9057528, 9057542, 9057554, 9057519, 9057544, 9002297, 9002378, 9002420, and 9003465). These spiders were examined using a Leica MZ 12 microscope with Leica Plan Apo 1.6× objective lens (MCZ IZ specimen 50966), optical and scanning electron microscopic (SEM) imaging (CASENT 9057540), and SEM imaging and embedded for microtoming. The spider's remains will be stored at the respective institutions.

Spiders were embedded and prepared using a standard preparation technique for microtoming. They were rehydrated in a stepwise fashion: sequentially from the original 70 to 50% (30 min) to 30% (40 min) and water (20 min). Then the tip of a blade was inserted between the two anterior spines and above the base of the pedicel before submerging the specimen in the following solutions: 4% paraformaldehyde, 1% glutaraldehyde, and 0.1 M HEPES overnight. The fixed spiders were washed with 0.1 M HEPES (10 min) three times and then four times by milliQ water (15 min) on ice and then dehydrated sequentially at a low temperature with increasing concentrations of ethanol beginning with 50% ethanol on ice (45 min), 70% ethanol at −20 °C (30 min), and 95% ethanol at −20 °C (30 min). Next, we infiltrated the spider sample with an ethanol/London Resin (LR) white mixture with increasing resin concentrations: 1:1 ethanol/LR white at −20 °C overnight, 7:3 ethanol/LR white at −20 °C for 1 h, and LR white at −20 °C for 1 h. For the final polymerization step, we put the spider specimen in an oven-dried gel capsule in LR white with her spines pointing down at −50 °C overnight in an oven (DX300 Yamato Gravity convection). Once polymerized, we removed the gel capsule, trimmed the resin block with a razor blade, and prepared slices using a Leica Ultratomicrotome UCT.

Utilizing the combination of serial microtoming and high-resolution serial-section electron microscopy (ssEM),[50] we sectioned

https://doi.org/10.1021/acsami.2c09546
ACS Appl. Mater. Interfaces 2022, 14, 32982−32993

the silvery region of a female *Phoroncidia rubroargentea* (Berland, 1913) abdomen and took the images for the physical slices as they were obtained. We sliced the specimen using a step length of 65 nm. The images of as-obtained cross-sections were taken by high-resolution scanning electron microscopy (SEM) imaging with a pixel size of 8 × 8 nm. To resolve the contradiction between high resolution and imaging size, the images for different parts of one physical slice were taken respectively.

4.2. Image Processing. In subsequent image processing for two- and three-dimensional structural characterizations, the different section images as obtained in Section 4.1 for one physical slice were stitched together to get a complete image for the physical slice. All the slice images were assigned to get the image series for the subject silvery region. The stitching and alignment were done in the TrakEM project in ImageJ.[51] This technique of automated serial sectioning in combination with electron microscopy has been successfully applied to the large volume nanoscale imaging of a broad range of materials systems, especially biological tissues and structures such as characterizing the brain. This technique allows researchers to resolve both individual features down to the nanoscale and 3D structural mapping of a large region.

The image segmentation was done in ImageJ for the three-dimensional structural characterizations, and the volume and surface rendering was realized in Avizo and Blender, respectively. The quantitative structural analyses were made using Avizo based on strict isolation and identification of each individual guanine crystal as one entity for statistical analyses.

4.3. Optical Modeling. The implementations of the 3D optical simulations in this work were all done using the finite-difference time-domain (FDTD) method and realized using the software Lumerical FDTD Solutions. The birefringence orientations were assigned to each guanine crystal separately in the simulation models. In the FDTD optical modeling, we used the plane wave of light in the BFAST mode, allowing light incidence at large angles, and the PML boundary condition. For the optical modeling in Figure 2B–D, the simulation time was set to be 10,000 fs for the optical modeling, the mesh accuracy was set to be 4, and the auto shut off min was set at 1e-06. For the optical modeling in Figure 2B, the box size was 2000 × 2000 × 6000 nm for the modeling with 5 layers, 2000 × 2000 × 7000 nm for the modeling with 10 layers, 2000 × 2000 × 9000 nm for the modeling with 20 layers, and 2000 × 2000 × 11 μm for the modeling with 30 layers. For the optical modeling in Figure 2C, the box size was 2000 × 2000 × 9000 nm. For the optical modeling in Figure 2E,F, the simulation time was set to be 1,000,000 fs for the simplified model 1 and 2, the mesh accuracy was set to be 5, and the auto shut off min was set to be at 1e-7. The size of the simulation box was 3000 × 3000 × 35,000 nm for the simplified model 1 and 3000 × 3000 × 58,000 nm for the simplified model 2. For the modeling in Figures 3–5, the size of the simulation box was 25 × 19 × 8 μm, the simulation time was set to be 1e12 fs, the mesh accuracy was set to be 5, and the auto shut off min was set at 1e-7.

■ ASSOCIATED CONTENT

Supporting Information

The Supporting Information is available free of charge at https://pubs.acs.org/doi/10.1021/acsami.2c09546.

Enlarged details on the guanine crystal assembly; the optical performance of the hypothetic nonbirefringent guanine component in the simplified models and true structures; schematic diagram for the optical modeling; the optical performance of the simplified model 2 under random crystallographic distribution of type 2 crystal; and electric field strength distributions for various wavelengths (PDF)

■ AUTHOR INFORMATION

Corresponding Authors

Fangfu Ye − *Oujiang Laboratory (Zhejiang Lab for Regenerative Medicine, Vision and Brain Health), and Wenzhou Institute, University of Chinese Academy of Sciences, Wenzhou, Zhejiang 325001, China;* orcid.org/0000-0003-1279-105X; Email: fye@iphy.ac.cn

Ling Li − *Department of Mechanical Engineering, Virginia Tech, Blacksburg, Virginia 24060, United States;* orcid.org/0000-0002-6741-9741; Email: lingl@vt.edu

Jianwei Shuai − *Department of Physics and Fujian Provincial Key Laboratory for Soft Functional Materials Research, Xiamen University, Xiamen, Fujian 361005, China; Oujiang Laboratory (Zhejiang Lab for Regenerative Medicine, Vision and Brain Health), and Wenzhou Institute, University of Chinese Academy of Sciences, Wenzhou, Zhejiang 325001, China; State Key Laboratory of Cellular Stress Biology, Innovation Center for Cell Signaling Network, and National Institute for Data Science in Health and Medicine, Xiamen University, Xiamen, Fujian 361102, China;* Email: jianweishuai@xmu.edu.cn

Authors

Jinjin Zhong − *Department of Physics, Xiamen University, Xiamen, Fujian 361005, China; Oujiang Laboratory (Zhejiang Lab for Regenerative Medicine, Vision and Brain Health), and Wenzhou Institute, University of Chinese Academy of Sciences, Wenzhou, Zhejiang 325001, China;* orcid.org/0000-0002-9782-9354

Zhengyong Song − *Department of Electronic Science, Xiamen University, Xiamen, Fujian 361005, China*

Long Zhang − *Department of Physics, Xiamen University, Xiamen, Fujian 361005, China*

Xiang Li − *Department of Physics, Xiamen University, Xiamen, Fujian 361005, China*

Qingzu He − *Department of Physics, Xiamen University, Xiamen, Fujian 361005, China*

Yuer Lu − *Department of Physics, Xiamen University, Xiamen, Fujian 361005, China*

Sarah Kariko − *Museum of Comparative Zoology, Harvard University, Cambridge, Massachusetts 02318, United States*

Peter Shaw − *Oujiang Laboratory (Zhejiang Lab for Regenerative Medicine, Vision and Brain Health), and Wenzhou Institute, University of Chinese Academy of Sciences, Wenzhou, Zhejiang 325001, China;* orcid.org/0000-0002-3187-8938

Liyu Liu − *Oujiang Laboratory (Zhejiang Lab for Regenerative Medicine, Vision and Brain Health), and Wenzhou Institute, University of Chinese Academy of Sciences, Wenzhou, Zhejiang 325001, China*

Complete contact information is available at: https://pubs.acs.org/10.1021/acsami.2c09546

Author Contributions

The manuscript was written through contributions of all authors. All authors have given approval to the final version of the manuscript.

Funding

This work is supported by the National Natural Science Foundation of China (Grants 11874310, and 12090052 to Shuai and 11974066 to Liu) and the China Postdoctoral Science Foundation (Grant 2016M602071 to Xiang Li).

Notes

The authors declare no competing financial interest.

■ ACKNOWLEDGMENTS

J.W.S. thanks Prof. Shuping Li from the Department of Physics, Xiamen University, for providing the software of Lumerical FDTD Solutions. L.L. acknowledges the support from the Department of Mechanical Engineering, Virginia Tech. The authors greatly acknowledge the technical support from Dr. Richard Schalek from Prof. Jeff W. Lichtman's research group at Harvard University for his kind assistance for the serial sectioning and electron microscopic imaging. S.J.K. acknowledges the support of the Invertebrate Zoology Collections, Museum of Comparative Zoology, and Curators Charles Griswold and Lauren Esposito as well as Darrell Ubick and Anthea Carmichael from the California Academy of Sciences for loaning specimens.

■ REFERENCES

(1) Weber, M. F.; Stover, C. A.; Gilbert, L. R.; Nevitt, T. J.; Ouderkirk, A. J. Giant Birefringent Optics in Multilayer Polymer Mirrors. *Science* **2000**, *287*, 2451−2456.
(2) Gur, D.; Palmer, B. A.; Weiner, S.; Addadi, L. Light Manipulation by Guanine Crystals in Organisms: Biogenic Scatterers, Mirrors, Multilayer Reflectors and Photonic Crystals. *Adv. Funct. Mater.* **2017**, *27*, 1603514.
(3) Thelen, A. Nonpolarizing Interference Films inside a Glass Cube. *Appl. Opt.* **1976**, *15*, 2983−2985.
(4) Thelen, A. Avoidance or Enhancement of Polarization in Multilayers. *JOSA* **1980**, *70*, 118−121.
(5) Lissberger, P. H. Optical Applications of Dielectric Thin Films. *Rep. Prog. Phys.* **1970**, *33*, 197.
(6) Banning, M. Practical Methods of Making and Using Multilayer Filters. *JOSA* **1947**, *37*, 792−797.
(7) Jordan, T. M.; Partridge, J. C.; Roberts, N. W. Non-Polarizing Broadband Multilayer Reflectors in Fish. *Nat. Photonics* **2012**, *6*, 759−763.
(8) Jordan, T. M.; Partridge, J.; Roberts, N. Disordered Animal Multilayer Reflectors and the Localization of Light. *J. R. Soc., Interface* **2014**, *11*, 20140948.
(9) Feller, K. D.; Jordan, T. M.; Wilby, D.; Roberts, N. W. Selection of the Intrinsic Polarization Properties of Animal Optical Materials Creates Enhanced Structural Reflectivity and Camouflage. *Philos. Trans. R. Soc., B* **2017**, *372*, 20160336.
(10) Jordan, T. M.; Partridge, J. C.; Roberts, N. W. Suppression of Brewster Delocalization Anomalies in an Alternating Isotropic-Birefringent Random Layered Medium. *Phys. Rev. B* **2013**, *88*, No. 041105.
(11) Gutman, A. B. Significance of Uric Acid as a Nitrogenous Waste in Vertebrate Evolution. *Arthritis Rheum.* **1965**, *8*, 614−626.
(12) Anderson, J. F. The Excreta of Spiders. *Comp. Biochem. Physiol.* **1966**, *17*, 973−982.
(13) Oxford, G. S.; Gillespie, R. G. Evolution and Ecology of Spider Coloration. *Annu. Rev. Entomol.* **1998**, *43*, 619−643.
(14) Levy-Lior, A.; Pokroy, B.; Levavi-Sivan, B.; Leiserowitz, L.; Weiner, S.; Addadi, L. Biogenic Guanine Crystals from the Skin of Fish May Be Designed to Enhance Light Reflectance. *Cryst. Growth Des.* **2008**, *8*, 507−511.
(15) Levy-Lior, A.; Shimoni, E.; Schwartz, O.; Gavish-Regev, E.; Oron, D.; Oxford, G.; Weiner, S.; Addadi, L. Guanine-Based Biogenic Photonic-Crystal Arrays in Fish and Spiders. *Adv. Funct. Mater.* **2010**, *20*, 320−329.
(16) Denton, E. J. Review Lecture: On the Organization of Reflecting Surfaces in Some Marine Animals. *Philos. Trans. R. Soc., B* **1970**, *258*, 285−313.
(17) Gur, D.; Leshem, B.; Pierantoni, M.; Farstey, V.; Oron, D.; Weiner, S.; Addadi, L. Structural Basis for the Brilliant Colors of the Sapphirinid Copepods. *J. Am. Chem. Soc.* **2015**, *137*, 8408−8411.
(18) Gur, D.; Palmer, B. A.; Leshem, B.; Oron, D.; Fratzl, P.; Weiner, S.; Addadi, L. The Mechanism of Color Change in the Neon Tetra Fish: A Light-Induced Tunable Photonic Crystal Array. *Angew. Chem., Int. Ed.* **2015**, *54*, 12426−12430.
(19) Denton, E.; Nicol, J. A Survey of Reflectivity in Silvery Teleosts. *J. Mar. Biol. Assoc. U. K.* **1966**, *46*, 685−722.
(20) Denton, E. J.; Gilpin-Brown, J. B.; Wright, P. G. The Angular Distribution of the Light Produced by Some Mesopelagic Fish in Relation to Their Camouflage. *Proc. R. Soc. London, Ser. B* **1972**, *182*, 145−158.
(21) Gur, D.; Leshem, B.; Farstey, V.; Oron, D.; Addadi, L.; Weiner, S. Light-Induced Color Change in the Sapphirinid Copepods: Tunable Photonic Crystals. *Adv. Funct. Mater.* **2016**, *26*, 1393−1399.
(22) Palmer, B. A.; Taylor, G. J.; Brumfeld, V.; Gur, D.; Shemesh, M.; Elad, N.; Osherov, A.; Oron, D.; Weiner, S.; Addadi, L. The Image-Forming Mirror in the Eye of the Scallop. *Science* **2017**, *358*, 1172−1175.
(23) Gur, D.; Nicolas, J. D.; Brumfeld, V.; Bar-Elli, O.; Oron, D.; Levkowitz, G. The Dual Functional Reflecting Iris of the Zebrafish. *Adv. Sci.* **2018**, *5*, 1800338.
(24) Dacke, M.; Nilsson, D.-E.; Warrant, E.; Blest, A.; Land, M.; O'carroll, D. Built-in Polarizers Form Part of a Compass Organ in Spiders. *Nature* **1999**, *401*, 470−473.
(25) Mueller, K. P.; Labhart, T. Polarizing Optics in a Spider Eye. *J. Comp. Physiol.* **2010**, *196*, 335−348.
(26) Kimura, T.; Takasaki, M.; Hatai, R.; Nagai, Y.; Uematsu, K.; Oaki, Y.; Osada, M.; Tsuda, H.; Ishigure, T.; Toyofuku, T.; Shimode, S.; Imai, H. Guanine Crystals Regulated by Chitin-Based Honeycomb Frameworks for Tunable Structural Colors of Sapphirinid Copepod, Sapphirina Nigromaculata. *Sci. Rep.* **2020**, *10*, 1−7.
(27) Gur, D.; Leshem, B.; Oron, D.; Weiner, S.; Addadi, L. The Structural Basis for Enhanced Silver Reflectance in Koi Fish Scale and Skin. *J. Am. Chem. Soc.* **2014**, *136*, 17236−17242.
(28) Oxford, G. In Guanine as a Colorant in Spiders: Development, Genetics, Phylogenetics and Ecology. In *Proceedings of the 17th European Colloquium of Arachnology*; British Arachnological Society: Edinburgh, 1997, 121−131.
(29) Hirsch, A.; Gur, D.; Polishchuk, I.; Levy, D.; Pokroy, B.; Cruz-Cabeza, A. J.; Addadi, L.; Kronik, L.; Leiserowitz, L. "Guanigma:" The Revised Structure of Biogenic Anhydrous Guanine. *Chem. Mater.* **2015**, *27*, 8289−8297.
(30) Thewalt, U.; Bugg, C.; Marsh, R. The Crystal Structure of Guanine Monohydrate. *Acta Crystallogr., Sect. B: Struct. Crystallogr. Cryst. Chem.* **1971**, *27*, 2358−2363.
(31) Guille, K.; Clegg, W. Anhydrous Guanine: A Synchrotron Study. *Acta Crystallogr., Sect. C: Cryst. Struct. Commun.* **2006**, *62*, o515−o517.
(32) Oaki, Y.; Kaneko, S.; Imai, H. Morphology and Orientation Control of Guanine Crystals: A Biogenic Architecture and Its Structure Mimetics. *J. Mater. Chem.* **2012**, *22*, 22686−22691.
(33) Gur, D.; Politi, Y.; Sivan, B.; Fratzl, P.; Weiner, S.; Addadi, L. Guanine-Based Photonic Crystals in Fish Scales Form from an Amorphous Precursor. *Angew. Chem., Int. Ed.* **2013**, *52*, 388−391.
(34) Gur, D.; Pierantoni, M.; Elool Dov, N.; Hirsh, A.; Feldman, Y.; Weiner, S.; Addadi, L. Guanine Crystallization in Aqueous Solutions Enables Control over Crystal Size and Polymorphism. *Cryst. Growth Des.* **2016**, *16*, 4975−4980.
(35) Chen, F.; Ma, Y.; Wang, Y.; Qi, L. A Novel Tautomeric Polymorph of Anhydrous Guanine and Its Reversible Water Harvesting Property. *Cryst. Growth Des.* **2018**, *18*, 6497−6503.
(36) Chen, F.; Wu, B.; Elad, N.; Gal, A.; Liu, Y.; Ma, Y.; Qi, L. Controlled Crystallization of Anhydrous Guanine B Nano-Platelets Via an Amorphous Precursor. *CrystEngComm* **2019**, *21*, 3586−3591.
(37) Land, M. A Multilayer Interference Reflector in the Eye of the Scallop, Pecten Maximus. *J. Exp. Biol.* **1966**, *45*, 433−447.

https://doi.org/10.1021/acsami.2c09546
ACS Appl. Mater. Interfaces 2022, 14, 32982−32993

(38) Denton, E. J.; Land, M. Mechanism of Reflexion in Silvery Layers of Fish and Cephalopods. *Proc. R. Soc. London, Ser. B* **1971**, *178*, 43−61.
(39) McKenzie, D. R.; Yin, Y.; McFall, W. D. Silvery Fish Skin as an Example of a Chaotic Reflector. *Proc. R. Soc. London, Ser. A* **1995**, *451*, 579−584.
(40) Partridge, J.; Douglas, R.; Marshall, N.; Chung, W.-S.; Jordan, T. M.; Wagner, H.-J. Reflecting Optics in the Diverticular Eye of a Deep-Sea Barreleye Fish (Rhynchohyalus Natalensis). *Proc. R. Soc. London, Ser. B* **2014**, *281*, 20133223.
(41) Denton, E.; Nicol, J. Polarization of Light Reflected from the Silvery Exterior of the Bleak, Alburnus Alburnus. *J. Mar. Biol. Assoc. U. K.* **1965**, *45*, 705−709.
(42) Rowe, D.; Denton, E. The Physical Basis of Reflective Communication between Fish, with Special Reference to the Horse Mackerel, Trachurus Trachurus. *Philos. Trans. R. Soc. London, Ser. B* **1997**, *352*, 531−549.
(43) Kariko, S.; Timonen, J. V.; Weaver, J. C.; Gur, D.; Marks, C.; Leiserowitz, L.; Kolle, M.; Li, L. Structural Origins of Coloration in the Spider Phoroncidia Rubroargentea Berland, 1913 (Araneae: Theridiidae) from Madagascar. *J. R. Soc., Interface* **2018**, *15*, 20170930.
(44) Wilts, B. D.; Michielsen, K.; De Raedt, H.; Stavenga, D. G. Sparkling Feather Reflections of a Bird-of-Paradise Explained by Finite-Difference Time-Domain Modeling. *Proc. Natl. Acad. Sci.* **2014**, *111*, 4363−4368.
(45) Hirsch, A.; Palmer, B. A.; Elad, N.; Gur, D.; Weiner, S.; Addadi, L.; Kronik, L.; Leiserowitz, L. Biologically Controlled Morphology and Twinning in Guanine Crystals. *Am. Ethnol.* **2017**, *129*, 9548−9552.
(46) Land, M. F. The Physics and Biology of Animal Reflectors. *Prog. Biophys. Mol. Biol.* **1972**, *24*, 75−106.
(47) Land, M. F.; Nilsson, D.-E. *Animal Eyes (Oxford Animal Biology Series)*; Oxford University Press: Oxford, 2002.
(48) Choi, S. H.; Kim, S.-W.; Ku, Z.; Visbal-Onufrak, M. A.; Kim, S.-R.; Choi, K.-H.; Ko, H.; Choi, W.; Urbas, A. M.; Goo, T.-W.; Kim, Y. L. Anderson Light Localization in Biological Nanostructures of Native Silk. *Nat. Commun.* **2018**, *9*, 1−14.
(49) Chinta, S. P.; Goller, S.; Uhl, G.; Schulz, S. Identification and Synthesis of Branched Wax-Type Esters, Novel Surface Lipids from the Spider Argyrodes Elevatus (Araneae: Theridiidae). *Chem. Biodiversity* **2016**, *13*, 1202−1220.
(50) Hildebrand, D. G. C.; Cicconet, M.; Torres, R. M.; Choi, W.; Quan, T. M.; Moon, J.; Wetzel, A. W.; Champion, A. S.; Graham, B. J.; Randlett, O. Whole-Brain Serial-Section Electron Microscopy in Larval Zebrafish. *Nature* **2017**, *545*, 345−349.
(51) Cardona, A.; Saalfeld, S.; Schindelin, J.; Arganda-Carreras, I.; Preibisch, S.; Longair, M.; Tomancak, P.; Hartenstein, V.; Douglas, R. J. Trakem2 Software for Neural Circuit Reconstruction. *PLoS One* **2012**, *7*, No. e38011.

https://doi.org/10.1021/acsami.2c09546
ACS Appl. Mater. Interfaces 2022, 14, 32982−32993